JOC The Journal of Organic Chemistry

Article

pubs.acs.org/joc

Origin of High *E*-Selectivity in 4-Pyrrolidinopyridine-Catalyzed Tetrasubstituted α,α′-Alkenediol: A Computational and Experimental Study

Masahiro Yamanaka,*[,†] Urara Yoshida,[†] Makoto Sato,[†] Takashi Shigeta,[‡] Keisuke Yoshida,[‡] Takumi Furuta,[‡] and Takeo Kawabata*[,‡]

[†]Department of Chemistry and Research Center for Smart Molecules, Faculty of Science, Rikkyo University, 3-34-1 Nishi-Ikebukuro, Toshima-ku, Tokyo 171-8501, Japan

[‡]Institute for Chemical Research, Kyoto University, Uji, Kyoto 611-0011, Japan

Supporting Information

ABSTRACT: We have developed 4-pyrrolidinopyridine catalysts for the geometry-selective (*E*-selective) acylation of tetrasubstituted α,α′-alkenediols. To elucidate the major factors of the high geometry selectivity, experimental and computational studies were carried out. The control experiments with respect to the substituent of the substrate indicated the fundamental hydrogen bonding of the acidic hydrogen of NHNs and the *Z*-OH in the substrate. Comparison between C_2- and C_1-symmetric catalysts exhibited the necessity of the C_2-symmetric catalyst structure. The computationally proposed transition state (TS) model well explained the experimental results. Whereas the fundamental NH/amide-CO and the two-point free-OH/acetate anion hydrogen bonds stabilize the transition state (TS), affording the *E*-product, the steric repulsion between the N-protecting group and the amide side chain destabilizes TS, affording the *Z*-product. The role of the two amide side chains of the catalyst in a C_2-symmetric fashion is the enhancement of the molecular recognition ability through the additional hydrogen bond in a cooperative manner.

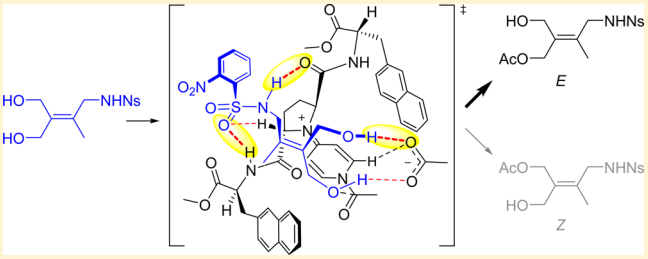

INTRODUCTION

The selective manipulation of multiple hydroxy groups of polyol compounds is a fundamental challenge in current organic synthesis.[1,2] We have developed numerous selective reactions, including the chemo- and regioselective acylation of glycopyranoses,[3] the chemoselective monoacylation of linear diols,[4] the chemoselective acylation of a secondary alcohol in the presence of a primary alcohol,[5] and the geometry-selective acylation of tetrasubstituted α,α′-alkenediols[6] by organocatalysis. In those reactions, the multiple hydrogen bonds between the C_2-symmetric 4-pyrrolidinopyridine catalysts (**1** and **2**) and the substrates play key roles in the molecular recognition depending on the substrate structure (Figure 1). In particular, the discrimination of the two hydroxy groups having intrinsically similar reactivity has been a difficult task.[7] Whereas the geometry-selective acylation of various unsymmetrically *trisubstituted* 2-alkylidene-1,3-propanediols and the deacylation of the corresponding diesters have been achieved by enzymatic methods,[8] the corresponding nonenzymatic method has been scarcely reported. We have reported the highly geometry-selective (*E*-selective) acylation of tri- and tetrasubstituted 2-alkylidene-1,3-propanediols **3** and **4** using **2** as the catalyst (Figure 2).[6] To the best of our knowledge, this is the only example of the highly geometry-selective acylation of tetrasubstituted

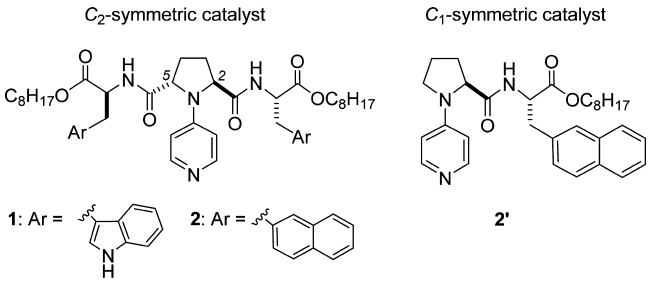

Figure 1. C_2- and C_1-symmetric 4-pyrrolidinopyridine catalysts.

2-alkylidene-1,3-propanediols among enzymatic and nonenzymatic methods.

We herein clarify the origin of the unprecedentedly high geometry selectivity and the role of the two amide side chains at C(2) and C(5) of **2** by experimental and computational studies. Focusing on the molecular recognition process through hydrogen-bonding interactions between **2** and tetrasubstituted alkenediols, the substituent effects of **4**, **5**, and **6** were investigated in detail (Figure 2). In addition, the molecular recognition ability of **2** and **2′** was experimentally and

Received: December 30, 2014
Published: February 12, 2015

DOI: 10.1021/jo5029453
J. Org. Chem. 2015, 80, 3075−3082

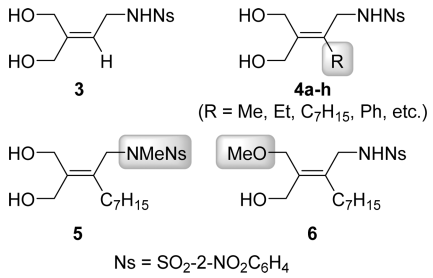

Figure 2. Tri- and tetrasubstituted 2-alkylidene-1,3-propanediols.

computationally compared to identify the necessity of the C_2-symmetric catalyst structure. The computationally proposed transition state (TS) model well explained the experimental results.

RESULTS AND DISCUSSION

Selected data for the catalytic acylation of various tetrasubstituted alkenediols **4** from our previous report[6] and additional new data (entries 8 and 12) are shown in Table 1. Remarkable differences in geometry selectivity depending on substituent R were observed in the present **2**-catalyzed acylation of **4**. Highly *E*-selective (96:4∼>99:<1) acylation (93−98%) was noted for **4a**−**4g** (entries 1−7). In contrast, nonselective acylation was observed in the catalytic acylation of phenyl-substituted alkenediol **4h** (*E*-**7**:*Z*-**7** = 50:50, entry 8). The high geometry selectivity in the acylation of **4b**−**4f** was associated with the high yield of the monoacylation (entries 2−6).[9] This indicates that the first acylation to give the monoacylate proceeded in an accelerative manner.[4,10,11] The high selectivity (98:2) was maintained even when the reaction was conducted in $CHCl_3$/DMF = 4:1 instead of $CHCl_3$, but the chemical yield was decreased (69%, entry 4 vs entry 9). On the other hand, use of pure DMF hampered the geometry selectivity (entry 4 vs entry 10). The experimental results suggest that the hydrogen-bonding interactions between **2** and **4** play a key role in the geometry-selective acylation and the smooth monoacylation through molecular recognition. To obtain the mechanistic insights with respect to the hydrogen-bonding network between **2** and **4**, substituent effects on the coordination sites of **4** were investigated. The use of NMeNs (Ns = 2-nitrobenzenesulfonyl) derivative **5** resulted in a significant decrease of the geometry selectivity and a diminished yield of the monoacylation (entry 11 vs entry 4). The relative acylation rate

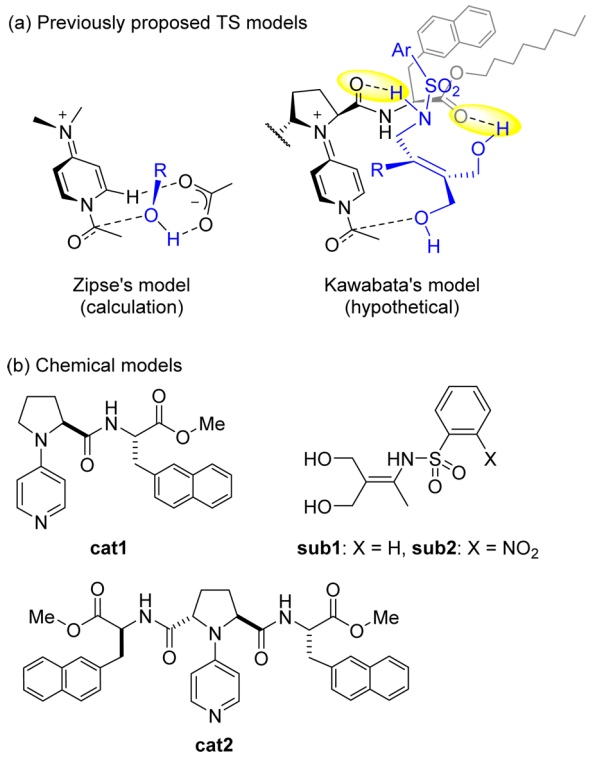

Figure 3. (a) Proposed TS models and (b) computational chemical models.

Table 1. Catalytic Acylation of Tetrasubstituted Alkenediols 4 in the Presence of 2

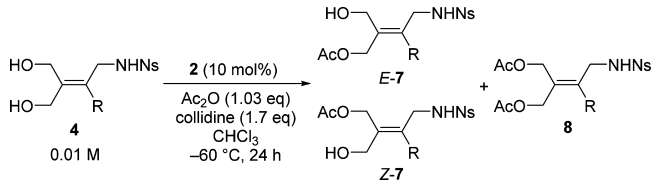

entry	R	4	7 [%]	*E*-7:*Z*-7[b]	8 [%]/recovery [%]
1	Me	**4a**	52	>99: <1	24/24
2	Et	**4b**	93	98:2	1/2
3	Pr	**4c**	96	98:2	∼0/3
4	C_7H_{15}	**4d**	98	98:2	∼0/1
5	$H_2CH_2CH{=}CH_2$	**4e**	97	98:2	∼0/3
6	CH_2Ph	**4f**	98	98:2	∼0/1
7[a]	Br	**4g**	73	96:4[b]	15/12
8	Ph	**4h**	55	50:50	15/15
9[c]	C_7H_{15}	**4d**	69	98:2	8/6
10[d]	C_7H_{15}	**4d**	41	50:50	14/36
11[e]	C_7H_{15}	**5**	64[f]	64:36[g]	
12[h]	C_7H_{15}	**4d**	97	93:7	

[a]Run in $CHCl_3$/THF (10:1). [b]*E*-**7g** and *Z*-**7g** (R = Br) indicate that NHNs and OAc are in *E*- and *Z*-geometry to each other, respectively, although this does not follow the nomenclature. [c]Run in $CHCl_3$/DMF (4:1). [d]Run in DMF. [e]The corresponding NMeNs derivative was used. [f]The yield of the corresponding NMeNs derivatives. [g]The ratio of the corresponding NMeNs derivatives. [h]Catalyst **2′** was used instead of **2**.

DOI: 10.1021/jo5029453
J. Org. Chem. 2015, 80, 3075−3082

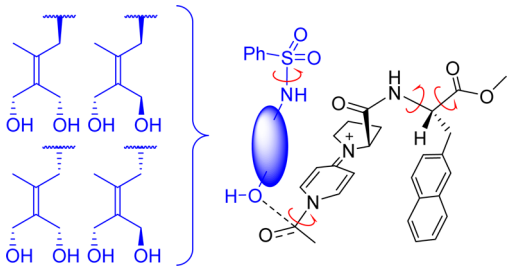

Figure 4. Conformational analysis of various TS models using **cat1**.

between **4d** and **5** (k_{4d}/k_5) was found to be 26 based on the competitive acylation reaction between them.[6] In addition, the acylation of **4d** was 89 times faster than that of the corresponding *Z*-OMe derivative **6** in the presence of **2** (k_{4d}/k_6 = 89).[6] Those substituent effects indicate that the acidic hydrogen of NHNs and the *Z*-OH in **4d**, which potentially act as hydrogen bond donors, are responsible for the *E*-selective acylation as well as the accelerative monoacylation of *E*-OH. The reaction of **4d** using the corresponding C_1-symmetric catalyst **2′** showed slightly lower selectivity than the C_2-symmetric one, but yet showed significantly high selectivity (*E*-7:*Z*-7 = 93:7, 97% yield of the monoacylation, entry 12).

Chemical Model and Computational Method. According to Zipse's computationally predicted mechanism[12] and our previously proposed mechanism,[6] the TS model of the nucleophilic attack of **4** on the *N*-acetylpyridinium ion of **2** was computationally investigated (Figure 3a). As the geometry selectivity was determined in the nucleophilic addition step, the diastereomeric TS models of this step (**TS-E** and **TS-Z**) leading to the *E*- and *Z*-acylation were compared. To obtain a mechanistic insight into the roles of the two amide side chains derived from α-amino-2-naphthalenepropanoic acid in a

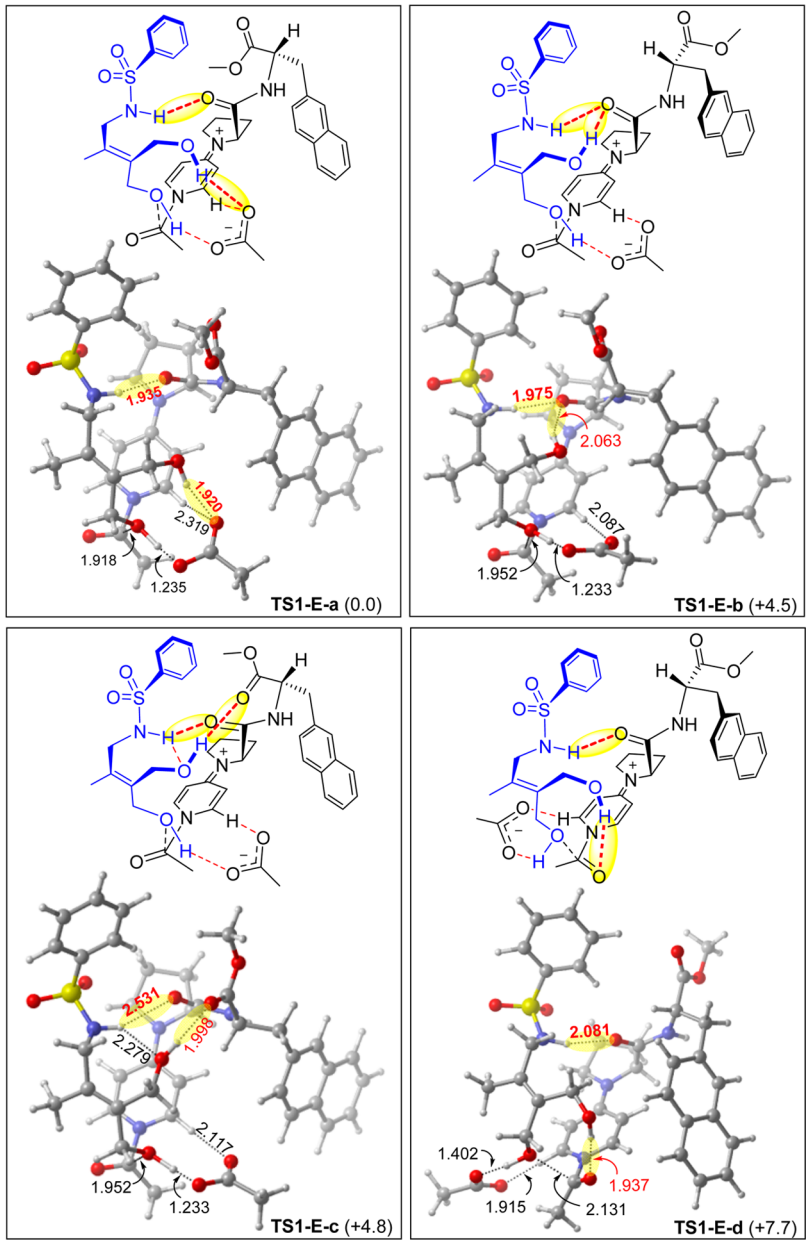

Figure 5. Schematic and 3D structures of typical diastereomeric TSs for **TS1-E**. Relative Gibbs free energies are shown in kcal/mol. Bond lengths are shown in Å.

DOI: 10.1021/jo5029453
J. Org. Chem. 2015, 80, 3075−3082

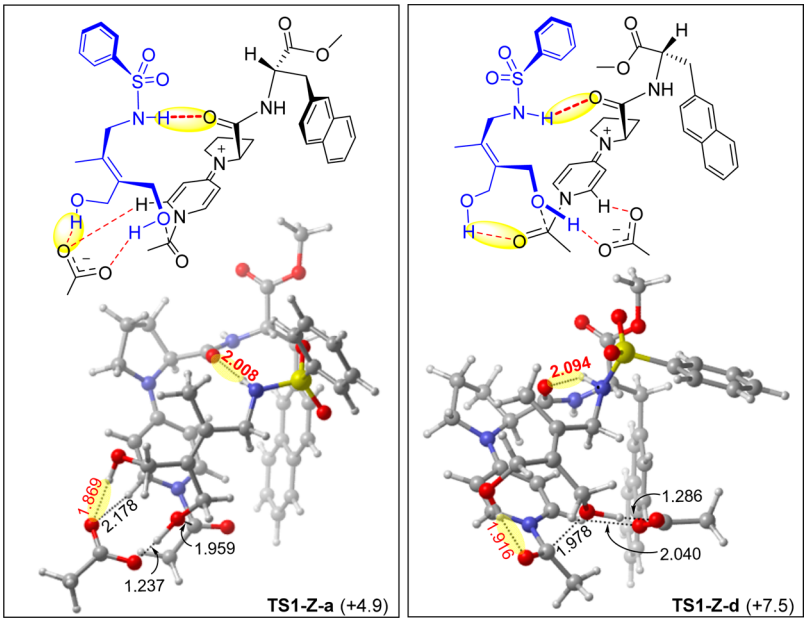

Figure 6. Schematic and 3D structures of typical diastereomeric TSs for **TS1-Z**. Relative Gibbs free energies are shown in kcal/mol. Bond lengths are shown in Å.

C_2-symmetric fashion, **cat1** (C_1 symmetry) and **cat2** (C_2 symmetry) were used as the chemical models of **2** (Figure 3b). In the chemical models of **cat1** and **cat2**, methyl ester was employed instead of octyl ester in the original catalyst structure to reduce computational cost, respectively. Focusing on the primary interactions (highlighted in yellow, Figure 3a) between the catalyst and the substrate for both **cat1** and **cat2**, the benzenesulfonyl group on the nitrogen substituent was initially employed instead of the Ns group in **sub1** to identify the most favored TS structure for geometry selectivity control. Based on the ideal TS structure, a more realistic chemical model of **sub2** bearing the NHNs group was also used to clarify the secondary effect of the NO_2 group in TS. All calculations were performed with the Gaussian 09 package.[13] Geometries were fully optimized and characterized by frequency calculation at the B3LYP/6-31G* level.[14,15] Gibbs free energies were also computed for the gas phase by single-point energy calculations at the same level.

There are a wide variety of conformational isomers for both the catalyst and the substrate because of their flexible linear structures (red curved arrows in Figure 4). To identify the fundamental interactions between the catalyst and the substrate, various diastereomeric TS models (**TS1**) using **cat1** and **sub1** were explored. As a preliminary conformational analysis, the relative Gibbs free energies of possible TS models having various types of hydrogen-bonding networks were compared to determine the energetically most favored TS structure. Using the totally optimized 31 TS models (**TS1-E**: 16 models, **TS1-Z**: 15 models; see the Supporting Information) as local minimum structures, diastereomeric TSs (series **a**–**d**) constructed by the typical hydrogen-bonding network are shown in Figures 5 (**TS1-E**) and 6 (**TS1-Z**).

On the basis of Zipse's computationally predicted TS model,[12] the nucleophilic OH group of **sub1** attacks the *N*-acylpyridinium ion while maintaining the interaction between the functional groups of **cat1** and the remaining OH group, and simultaneously the acetate anion abstracts the proton of the nucleophilic OH group. The hydrogen bond between the NH group of **sub1** and the amide carbonyl (amide-CO) of **cat1** plays a key role in the TS stabilization. It is supposed that the acidic NH group on the N-protecting phenylsulfonyl group of **sub1** forms an NH/amide-CO hydrogen bond as a fundamental interaction between **sub1** and *N*-acylpyridinium ion. In addition to this fundamental hydrogen bond, other hydrogen bonds formed between the remaining OH (free-OH) of **sub1** and the negatively charged sites of *N*-acylpyridinium ion (e.g., acyl and ester carbonyl groups) or acetate anion also affect the stabilization of TS (highlighted in yellow, Figures 5 and 6).[16] The most stable **TS1-E-a** has a strong NH/amide-CO hydrogen bond (1.935 Å) and two-point hydrogen bonds between the two OH groups of **sub1** and the acetate anion (1.235 Å, 1.920 Å). The two-point hydrogen bonds formed between the two OH groups and the anionic site enhance the stability of **TS1-E-a** (Figure 5). In contrast, free-OH interacts with amide-CO (2.063 Å) while keeping the strong NH/amide-CO hydrogen bond (1.975 Å) in **TS1-E-b**. However, **TS1-E-b** is 4.5-kcal/mol less stable than **TS1-E-a** due to the relatively weak hydrogen bond formed between free-OH and neutral amide-CO. Although **TS1-E-c** is our previously proposed TS model where the ester group of **cat1** (ester-CO) interacts with free-OH, it is 4.8-kcal/mol less stable than **TS1-E-a**. The ester-CO/free-OH hydrogen bond (1.998 Å) geometrically induces the intramolecular NH/free-OH hydrogen bond (2.279 Å) to significantly weaken the NH/amide-CO hydrogen bond (2.531 Å) in **TS1-E-c**. Such changes in the internal hydrogen-bonding network between **sub1** and **cat1** destabilize **TS1-E-c**. The other scenario involving the hydrogen bonding of free-OH stabilizes the developing negative charge of the *N*-acylpyridinium carbonyl group (acyl-CO) in TS (**TS1-E-d**). However, **TS1-E-d** is 7.7-kcal/mol higher in energy than **TS1-E-a** and an energetically disfavored TS. Whereas **TS1-Z** also has the fundamental NH/amide-CO hydrogen bond in a manner similar to **TS1-E**, only two series (**a** and **d**) of the hydrogen-bonding network enable to be constructed due to the geometrical requirement of the *Z*-selective acylation in **TS1-Z** (Figure 6). In both **TS1-Z-a**

DOI: 10.1021/jo5029453
J. Org. Chem. 2015, 80, 3075−3082

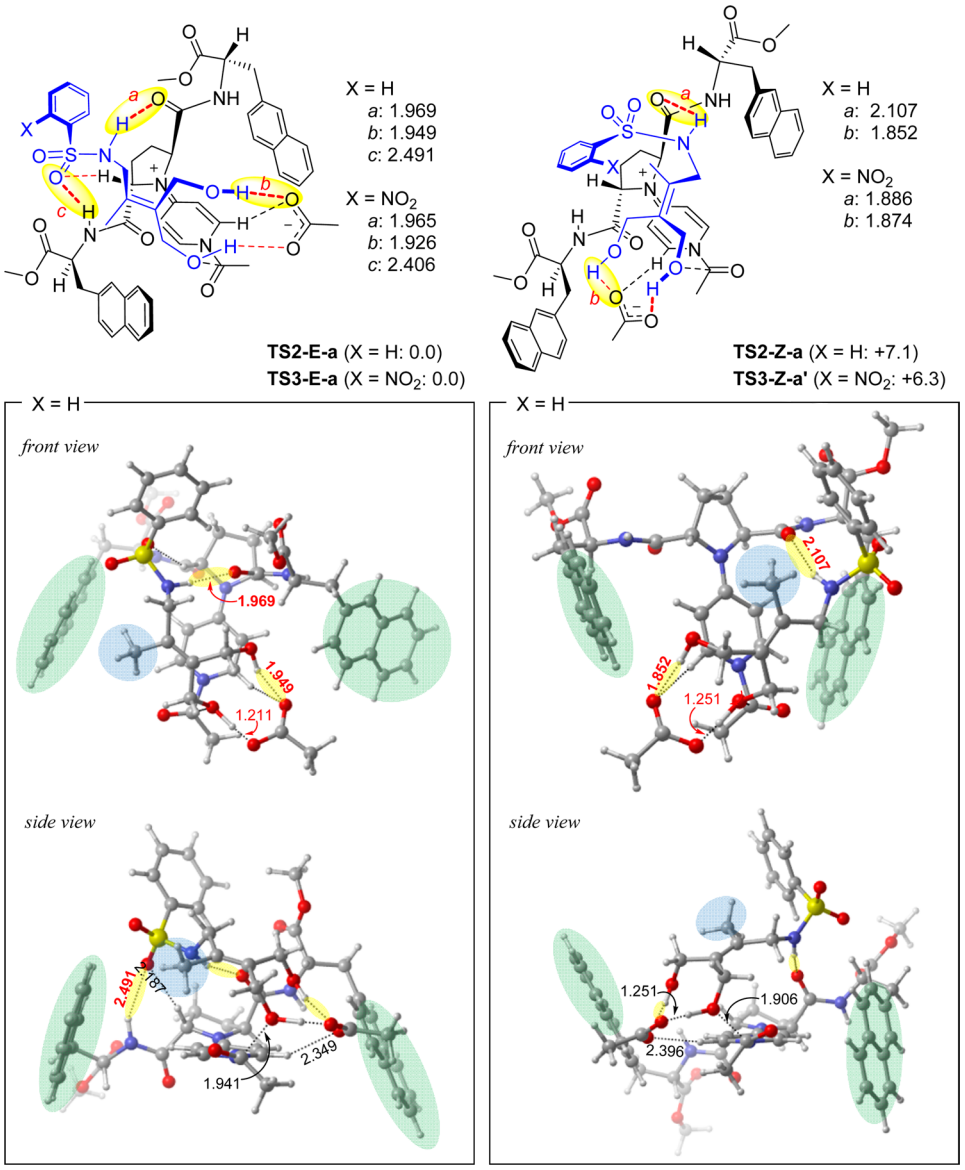

Figure 7. Schematic and 3D structures of diastereomeric TSs for **cat2**. Relative Gibbs free energies are shown in kcal/mol. Bond lengths are shown in Å.

and **TS1-Z-d**, the N-protecting phenylsulfonyl group is located close to the sterically demanding amide side chain of **cat1** to induce a large steric repulsion. **TS1-Z-a** having the two-point hydrogen bonds between the two OH groups of **sub1** and the acetate anion (1.237 Å, 1.869 Å) is energetically more favored than **TS1-Z-d** having the free-OH/acyl-CO hydrogen bond (1.916 Å). The relative Gibbs free energy difference between the most stable **TS1-E** and **TS1-Z** (e.g., **TS1-E-a** and **TS1-Z-a**) is qualitatively consistent with the experimental results in an *E*-selective manner.

After exploring **TS1** using **cat1** and **sub1**, the ideal TS structures were found to be **TS1-E-a** and **TS1-Z-a**, where the NH group and the free-OH of **sub1** interact with amide-CO and acetate anion, respectively, and the 2-naphthyl group is located far from **sub1** as the stable conformation of the amide side chain. On the basis of these promising TS structures, more realistic TS models (**TS2**) using C_2-symmetric **cat2** were investigated to elucidate the role of the two amide side chains. In addition, a more realistic chemical model of **sub2** bearing the NHNs group was also studied to identify the secondary effect of the NO_2 group in TS (**TS3**). By expanding **TS1-E-a** and **TS1-Z-a**, the realistic TS models (**TS2-E-a**, **TS2-Z-a**, **TS3-E-a**, and **TS3-Z-a**) were geometrically optimized, respectively (Figure 7). The relative Gibbs free energies between **TS-E** and **TS-Z** were significantly increased for **TS2** (7.1 kcal/mol) and **TS3** (6.9 kcal/mol) compared to **TS1** (4.9 kcal/mol). This is in qualitatively good agreement with the experimental results where C_2-symmetric **2** achieved higher *E*-selectivity (*E*:*Z* = 98:2) than C_1-symmetric **2′** (*E*:*Z* = 93:7). The gross structure and the hydrogen-bonding network in the right-hand part of **TS2-E-a** and **TS2-Z-a** are almost the same as those of **TS1-E-a** and **TS1-Z-a**, respectively (Figure 7). Both **TS2-E-a** and **TS2-Z-a** also have the NH/amide-CO hydrogen bond and the two-point free-OH/acetate anion hydrogen bonds as fundamental interactions stabilizing TS (highlighted in yellow). As for **TS2-E-a**, it is noted that the NH group of the additional amide side chain (amide-NH, left-hand part in **TS2-E-a**) interacts with the sulfonyl group of **sub1** (SO_2) to enhance the stabilization of TS (highlighted in yellow). This indicates that **cat2** possesses the dual function of the two amide side chains, albeit in a

DOI: 10.1021/jo5029453
J. Org. Chem. 2015, 80, 3075−3082

C_2-symmetric fashion. The induced-fit-type structural change of **cat2** caused by the multiple hydrogen-bonding interactions enables geometrical recognition. In contrast, the C_2-symmetric structure of **cat2** has no impact on the stability of **TS2-Z-a** because no additional interaction exists other than the fundamental interactions in **cat1** (Figure 7). Therefore, the additional SO_2/amide-NH hydrogen bond significantly stabilizes **TS2-E-a** and increases the relative Gibbs free energy difference between **TS2-E-a** and **TS2-Z-a** to achieve higher *E*-selectivity for **2** than **2′**. Focusing on the structural feature of **TS2**, the Me group of **sub1** in **TS2-E-a** (highlighted in blue) is located close to the additional amide side chain (highlighted in green, Figure 7). It is clear that the sterically demanding substituent (e.g., Ph) of the substrate induces a large steric repulsion with the additional amide side chain. In fact, phenyl-substituted alkenediol **4h** showed no geometry selectivity (*E*:*Z* = 50:50 in Table 1). The introduction of the N-protecting Ns group (**TS3-E-a** and **TS3-Z-a**) has little influence on the gross structures, the hydrogen-bonding network, and the relative Gibbs free energies of both **TS2-E-a** and **TS2-Z-a**. As the secondary effect of the NO_2 group in **TS3**, fundamental hydrogen bonds tend to be enhanced in comparison with **TS2**.

CONCLUSION

Experimental and DFT studies of the 4-pyrrolidinopyridine-catalyzed geometry-selective acylation of tetrasubstituted α,α'-alkenediols were carried out to reveal the major factors affecting *E*-selectivity, particularly the role of the two amide side chains of the catalyst in a C_2-symmetric fashion. Experiments comparing C_1-symmetric and C_2-symmetric catalysts showed that the geometry selectivity was sufficiently achieved even by the C_1-symmetric unit of the catalyst, and the additional amide side chain of the C_2-symmetric unit enhanced the stereocontrol ability. A mechanistic insight into the role played by the two amide side chains of the catalyst was obtained by DFT calculations. The fundamental NH/amide-CO and the two-point free-OH/acetate anion hydrogen bonds as well as the steric repulsion between the N-protecting group and the amide side chain mainly contribute to the *E*-selective acylation. The other amide side chain of the catalyst acts cooperatively to further stabilize TS of the *E*-selective acylation through the additional hydrogen bond, thereby achieving higher *E*-selectivity. The dual function of the amide side chains is responsible for the molecular recognition process. Each of them participates independently and in a cooperative manner in the events to achieve high geometry selectivity in the tetrasubstituted α,α'-alkenediols.

EXPERIMENTAL SECTION

General Remarks. ^{1}H and ^{13}C NMR spectra were obtained at 400 and 600 MHz, respectively, with chemical shifts being given in ppm units (tetramethylsilane as internal standards, indicating 0). IR spectra were recorded on an FT-IR spectrometer. Specific rotation was measured with an automatic digital polarimeter. MS spectra were recorded by a FAB mass spectrometer. TLC analysis and preparative TLC were performed on commercial glass plates bearing a 0.25 mm layer or 0.5 mm layer of silica gel. Silica gel chromatography was performed with 150−325 mesh silica gel. Dry solvents (dichloromethane, and chloroform; <50 ppm water contents) obtained from commercial suppliers were used without further purification.

Synthesis of Octyl (*S*)-3-(Naphthalen-2-yl)-2-((*S*)-1-(pyridin-4-yl)-pyrrolidine-2-carboxamido)propanoate (2′). To a solution of octyl (*S*)-2-amino-3-(naphthalen-2-yl)propanoate hydrochloride (406 μL, 0.57 mmol), *N*-(4-pyridyl)-L-proline[17] (189 mg, 0.38 mmol) in CH_2Cl_2 (5 mL) were added EDCI (109 mg, 0.57 mmol), HOBt (78 mg, 0.57 mmol) and NMM (115 mg, 1.14 mmol). After being stirred for 24 h, the mixture was diluted with EtOAc and washed with sat. aq. $NaHCO_3$ and brine, dried over $MgSO_4$, filtered, and evaporated in vacuo. The residue was purified by column chromatography to afford PPY-catalyst **2′** in 34% (142 mg) as a colorless powder.

Octyl (S)-3-(Naphthalen-2-yl)-2-((S)-1-(pyridin-4-yl)pyrrolidine-2-carboxamido)propanoate (2′).

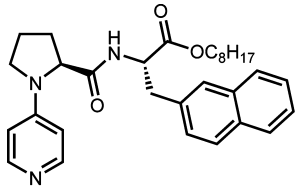

2′

mp 60−61 °C. $[\alpha]_{20}^{D}$ = −132 (c 0.32, $CHCl_3$). ^{1}H NMR (400 MHz, $CDCl_3$) δ 0.88 (t, *J* = 6.9 Hz, 3H), 1.22−1.29 (m, 9H), 1.50−1.58 (m, 3H), 1.79−1.85 (m, 1H), 2.06−2.18 (m, 3H), 3.08−3.15 (m, 1H), 3.20 (dd, *J* = 7.1, 14.0 Hz, 1H), 3.32 (t, *J* = 8.5 Hz, 1H), 3.39 (dd, *J* = 5.7, 14.0 Hz, 1H), 4.01 (dd, *J* = 2.8, 8.2 Hz, 1H), 4.06 (t, *J* = 6.9 Hz, 2H), 4.88 (q, *J* = 6.9 Hz, 1H), 6.31−6.33 (m, 2H), 6.55 (d, *J* = 7.3 Hz, 1H), 7.20 (dd, *J* = 1.6, 8.5 Hz, 1H), 7.44−7.50 (m, 3H), 7.71−7.75 (m, 2H), 7.79−7.82 (m, 1H), 8.14−8.15 (m, 1H). ^{13}C NMR (100 MHz, $CDCl_3$) δ 14.1, 22.6, 23.3, 25.7, 28.4, 29.1, 31.0, 31.7, 37.7, 48.4, 52.8, 63.1, 65.9, 108.0, 125.9, 126.4, 126.9, 127.3, 127.7, 127.9, 128.4, 132.4, 133.2, 133.3, 149.8, 151.7, 170.9, 172.0. IR (KBr) 3331, 2954, 2927, 1753, 1657, 1601, 1541, 1515 cm^{-1}. MS (FAB) *m*/*z* 502 $(M + H)^+$. HRMS (FAB) *m*/*z* calcd for $C_{31}H_{40}O_3N_3$ $(M + H)^+$ 502.3070, found 502.3069.

Procedure for Competitive Acylation Reaction between 4d/4h. According to our previous report,[6] the reaction was carried out as written below.

To a solution of *N*-(2-(1,3-dihydroxypropan-2-ylidene)nonyl)-2-nitrobenzenesulfonamide (12 mg, 1.0 equiv) and *N*-(4-hydroxy-3-(hydroxymethyl)-2-phenylbut-2-en-1-yl)-2-nitrobenzenesulfonamide (11 mg, 1.0 equiv), catalyst (1.5 mg, 10 mol %) and 2,4,6-collidine (6.6 μL, 1.7 equiv) in $CHCl_3$ (2.9 mL, concentration of the substrate: 0.01 M) was added acid anhydride (0.53 M solution in $CHCl_3$) (58 μL, 1.05 equiv) at −60 °C. The resulting mixture was stirred at the same temperature for 24 h. The reaction was quenched with MeOH (1 mL), and the solvent was evaporated. The residue was dissolved in EtOAc, washed with 1 N HCl and brine, dried over $MgSO_4$, filtered, and concentrated in vacuo. The crude compound was purified by preparative TLC (SiO_2, hexane:EtOAc = 1:3) to afford monoacylates **7h** in 20% (2.5 mg, *E*:*Z* = 57:43) and **7d** in 76% (9.8 mg, *E*:*Z* = 95:5). *E*/*Z* ratio of monoacylate **7h** was determined by the integration of ^{1}H NMR. Spectral data for compounds **7d** and **8d** were reported in our previous report.[6]

(E)-2-(Hydroxymethyl)-4-((2-nitrophenyl)sulfonamido)-3-phenylbut-2-en-1-yl Acetate) (E-7h).

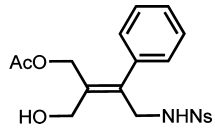

Colorless oil. ^{1}H NMR (400 MHz, $CDCl_3$) δ 2.04 (s, 3H), 2.25 (t, *J* = 5.5 Hz, 1H), 4.24 (d, *J* = 6.4 Hz, 2H), 4.39 (d, *J* = 5.5 Hz, 2H), 4.49 (s, 1H), 5.61 (t, *J* = 5.7 Hz, 1H), 6.88−6.90 (m, 2H), 7.20−7.24 (m, 3H), 7.67−7.74 (m, 2H), 7.81−7.84 (m, 1H), 8.02−8.04 (m, 1H). ^{13}C NMR (150 MHz, $CDCl_3$) δ 20.9, 45.9, 59.6, 63.6, 125.4, 128.18, 128.23, 128.6, 130.8, 132.9, 133.4, 134.1, 134.6, 137.6, 139.9, 170.9. IR (KBr) 3610, 3375, 3031, 2927, 1736, 1543 cm^{-1}. MS (FAB) *m*/*z* 443 $(M + Na)^+$. HRMS (FAB) *m*/*z* calcd for $C_{19}H_{20}O_7N_2SNa$ $(M + Na)^+$ 443.0889, found 443.0886.

(*E*)-Stereochemistry was determined by NOESY spectra as shown below.

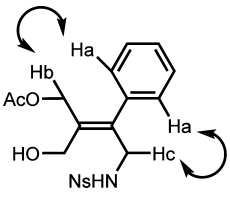

DOI: 10.1021/jo5029453
J. Org. Chem. 2015, 80, 3075−3082

*(Z)-2-(Hydroxymethyl)-4-((2-nitrophenyl)sulfonamido)-3-phenylbut-2-en-1-yl Acetate) (**Z-7h**).*

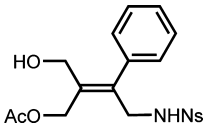

Colorless oil. ^{1}H NMR (600 MHz, $CDCl_3$) δ 1.90 (t, J = 5.9 Hz, 1H), 2.17 (s, 3H), 3.95 (d, J = 5.5 Hz, 2H), 4.26 (d, J = 5.5 Hz, 2H), 4.95 (s, 2H), 5.54 (t, J = 5.9 Hz, 1H), 6.89−6.91 (m, 2H), 7.16−7.22 (m, 3H), 7.64−7.70 (m, 2H), 7.80 (dd, J = 7.6 Hz, J = 1.4 Hz, 1H), 7.95 (dd, J = 1.4, 7.6 Hz, 1H). ^{13}C NMR (100 MHz, $CDCl_3$) δ 21.1, 45.9, 61.1, 61.5, 125.4, 125.4, 128.2, 128.5, 130.7, 132.9, 133.3, 134.2, 134.7, 137.4, 139.3, 1731.4. IR (KBr) 3617, 3371, 2960, 2925, 1730, 1714, 1543, 1412 cm^{-1}. MS (FAB) m/z 443 (M + Na)$^+$. HRMS (FAB) m/z calcd for $C_{19}H_{20}O_7N_2SNa$ (M + Na)$^+$ 443.0889, found 443.0887.

*2-(2-((2-Nitrophenyl)sulfonamido)-1-phenylethylidene)propane-1,3-diyl Diacetate (**8h**).*

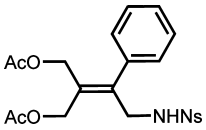

Colorless powder. mp 97−99 °C. ^{1}H NMR (400 MHz, $CDCl_3$) δ 2.02 (s, 3H), 2.13 (s, 3H), 4.27 (d, J = 6.0 Hz, 2H), 4.40 (s, 2H), 4.85 (s, 2H), 5.58 (t, J = 5.5 Hz, 1H), 6.88 (dd, J = 1.6, 8.0 Hz, 2H), 7.16−7.26 (m, 3H), 7.63−7.72 (m, 2H), 7.81 (dd, J = 1.4, 7.8 Hz, 1H), 7.96 (dd, J = 1.6, 7.6 Hz, 1H). ^{13}C NMR (100 MHz, $CDCl_3$) δ 20.8, 20.9, 45.9, 60.6, 62.9, 125.4, 128.1, 128.4, 128.6, 130.2, 130.7, 132.9, 133.3, 134.2, 137.1, 141.8, 147.6, 170.5, 170.9. IR (KBr) 1730, 1539, 1339, 1250 cm^{-1}. MS (FAB) m/z 485 (M + Na)$^+$. HRMS (FAB) m/z calcd for $C_{21}H_{22}O_8N_2SNa$ (M + Na)$^+$ 485.0995, found 485.0992.

*N-(4-Hydroxy-3-(hydroxymethyl)-2-phenylbut-2-en-1-yl)-2-nitrobenzenesulfonamide (**4h**).*

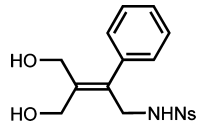

Colorless powder. mp 115−116 °C. ^{1}H NMR (400 MHz, $CDCl_3$) δ 1.97 (s, 1H), 2.44 (s, 1H), 4.08 (s, 2H), 4.21 (d, J = 6.0 Hz, 2H), 4.56 (s, 2H), 5.60 (t, J = 5.5 Hz, 1H), 6.88−6.90 (m, 2H), 7.18−7.23 (m, 3H), 7.69−7.75 (m, 2H), 7.81−7.83 (m, 1H), 8.05−8.07 (m, 1H). ^{13}C NMR (100 MHz, $CDCl_3$) δ 45.7, 61.4, 63.3, 125.5, 128.1, 128.4, 128.6, 131.0, 133.1, 133.5, 134.2, 136.4, 137.9, 138.0. IR (KBr) 2362, 1539, 1404, 1363 cm^{-1}. MS (FAB) m/z 401 (M + Na)$^+$. HRMS calcd for $C_{17}H_{18}O_6N_2SNa$ (M + Na)$^+$ 401.0783, found 401.0783.

■ ASSOCIATED CONTENT

Ⓢ Supporting Information

Copies of ^{1}H and ^{13}C spectra and computational details (Cartesian coordinates and absolute energies for stationary points). This material is available free of charge via the Internet at http://pubs.acs.org.

■ AUTHOR INFORMATION

Corresponding Authors

*E-mail: myamanak@rikkyo.ac.jp (M.Y.).
*E-mail: kawabata@scl.kyoto-u.ac.jp (T.K.).

Notes

The authors declare no competing financial interest.

■ ACKNOWLEDGMENTS

This work was supported by a Grant-in-Aid for Scientific Research on Innovative Areas "Advanced Molecular Transformations by Organocatalysts" from The Ministry of Education, Culture, Sports, Science and Technology, Japan, MEXT-Supported Program for the Strategic Research Foundation at Private Universities, and the Collaborative Research Program of Institute for Chemical Research, Kyoto University (No. 2014-82).

■ REFERENCES

(1) For nonenzymatic approaches to the regioselective acylation of carbohydrates, see: (a) Kurahashi, T.; Mizutani, T.; Yoshida, J. *J. Chem. Soc. Perkin Trans. 1* **1999**, 465−473. (b) Kurahashi, T.; Mizutani, T.; Yoshida, J. *Tetrahedron* **2002**, *58*, 8669−8677. (c) Griswold, K. S.; Miller, S. J. *Tetrahedron* **2003**, *59*, 8869−8875. (d) Kattnig, E.; Albert, M. *Org. Lett.* **2004**, *6*, 945−948. (e) Demizu, Y.; Kubo, Y.; Miyoshi, H.; Maki, T.; Matsumura, Y.; Moriyama, N.; Onomura, O. *Org. Lett.* **2008**, *10*, 5075−5077.

(2) The regioselective acylation of polyol derivatives via a molecular recognition process by peptide-based catalysts has been reported. For examples, see: (a) ref 1c. (b) Lewis, C. A.; Miller, S. J. *Angew. Chem., Int. Ed.* **2006**, *45*, 5616−5619. (c) Lewis, C. A.; Longcore, K. E.; Miller, S. J.; Wender, P. A. *J. Nat. Prod.* **2009**, *72*, 1864−1869.

(3) (a) Kawabata, T.; Muramatsu, W.; Nishio, T.; Shibata, T.; Schedel, H. *J. Am. Chem. Soc.* **2007**, *129*, 12890−12895. (b) Ueda, Y.; Muramatsu, W.; Mishiro, K.; Furuta, T.; Kawabata, T. *J. Org. Chem.* **2009**, *74*, 8802−8805.

(4) Yoshida, K.; Furuta, T.; Kawabata, T. *Angew. Chem., Int. Ed.* **2011**, *50*, 4888−4892.

(5) Yoshida, K.; Shigeta, T.; Furuta, T.; Kawabata, T. *Chem. Commun.* **2012**, *48*, 6981−6983.

(6) Yoshida, K.; Mishiro, K.; Ueda, Y.; Shigeta, T.; Furuta, T.; Kawabata, T. *Adv. Syn. Catal.* **2012**, *354*, 3291−3298.

(7) For an example of the discrimination of prochiral primary diols by peptide-based catalysts, see: Lewis, C. A.; Sculimbrene, B. R.; Xu, Y.; Miller, S. J. *Org. Lett.* **2005**, *7*, 3021−3023.

(8) (a) Schirmeister, T.; Otto, H.-H. *J. Org. Chem.* **1993**, *58*, 4819−4822. (b) Takabe, K.; Mase, N.; Hisano, T.; Yoda, H. *Tetrahedon Lett.* **2003**, *44*, 3267−3269. (c) Hisano, T.; Onodera, K.; Toyabe, Y.; Mase, N.; Yoda, H.; Takabe, K. *Tetrahedron Lett.* **2005**, *46*, 6293−6295. (d) Miura, T.; Kawashima, Y.; Umetsu, S.; Kanamori, D.; Tsuyama, N.; Jyo, Y.; Murakami, Y.; Imai, N. *Chem. Lett.* **2007**, *36*, 814−815. (e) Miura, T.; Kawashima, Y.; Takahashi, M.; Murakami, Y.; Imai, N. *Synth. Commun.* **2007**, *37*, 3105−3109. (f) Miura, T.; Okazaki, K.; Ogawa, K.; Otomo, E.; Umetsu, S.; Takahashi, M.; Kawashima, Y.; Jyo, Y.; Koyata, N.; Murakami, Y.; Imai, N. *Synthesis* **2008**, 2695−2700. (g) Miura, T.; Umetsu, S.; Kanamori, D.; Tsuyama, N.; Jyo, Y.; Kawashima, Y.; Koyata, N.; Murakami, Y.; Imai, N. *Tetrahedon* **2008**, *64*, 9305−9308.

(9) Among substrates **4a**−**4g** that underwent highly *E*-selective acylation, **4a** (R = Me) and **4g** (R = Br) gave monoacylates in moderate yields together with significant amounts of diacylates. This was assumed to be a result of the relatively poor solubility of those substrates in $CHCl_3$ at low temperature.

(10) The importance of the accelerative nature in the selective acylation and sulfonylation reactions has been noted. See: (a) Copeland, G. T.; Miller, S. J. *J. Am. Chem. Soc.* **2001**, *123*, 6496−6502. (b) Fiori, K. W.; Puchlopek, A. L. A.; Miller, S. J. *Nat. Chem.* **2009**, *1*, 630−634.

(11) The relative rate of acylation between **4d** and **4h** was determined to be k_{4d}/k_{4h} = 6.4 by the competitive acylation (see the Supporting Information). This suggests that *selective* substrates undergo acylation faster than *nonselective* substrates.

(12) Xu, S.; Held, I.; Kempf, B.; Mayr, H.; Steglich, W.; Zipse, H. *Chem.—Eur. J.* **2005**, *11*, 4751−4757.

(13) Frisch, M. J.; et al. *Gaussian 09*, Revision D.01.; Gaussian, Inc.:Wallingford, CT, 2013.

(14) (a) Becke, A. D. *J. Chem. Phys.* **1993**, *98*, 5648−5652. (b) Lee, C.; Yang, W.; Parr, R. G. *Phys. Rev. B* **1988**, *37*, 785−789.

(15) Hehre, W. J.; Radom, L.; Schleyer, P. v. R.; Pople, J. A. *Ab Initio Molecular Orbital Theory*; John Wiley: New York, 1986. References cited therein.

DOI: 10.1021/jo5029453
J. Org. Chem. 2015, 80, 3075−3082

(16) Hydrogen bonding networks affect the stabilization of TS even though some hydrogen bonds have a slightly longer distance than the usual one. See: (a) Steiner, T. *Angew. Chem., Int. Ed.* **2002**, *41*, 48−76. (b) Scheiner, S. *Hydrogen Bonding: A Theoretical Perspective*; Oxford University Press: New York, 1997.
(17) Edward, J. D.; Leigh, E. W.; Irving, M. K. *J. Am. Chem. Soc.* **1982**, *104*, 799−807.

DOI: 10.1021/jo5029453
J. Org. Chem. 2015, 80, 3075−3082